The Meteoritical Society

Meteoritics & Planetary Science 41, Nr 12, 1929–1945 (2006)
Abstract available online at http://meteoritics.org

Mobile element analysis by secondary ion mass spectrometry (SIMS) of impactite matrix samples from the Yaxcopoil-1 drill core in the Chicxulub impact structure

Horton E. NEWSOM[1*], Melissa J. NELSON[1], Charles K. SHEARER[1], and Burkhard O. DRESSLER[2]

[1]Institute of Meteoritics, Department of Earth and Planetary Sciences, Albuquerque, New Mexico 87131, USA
[2]5481 Oceanview Terrace, Nanaimo, British Columbia, V9V 1G7, Canada
[*]Corresponding author. E-mail: newsom@unm.edu

(Received 25 February 2005; revision accepted 29 September 2006)

Abstract–The concentrations of the fluid mobile trace elements lithium, beryllium, boron, and barium were measured in samples of the altered matrix of several impactite breccias of the Yaxcopoil-1 drill core using secondary ion mass spectrometry (SIMS) to determine the extent of transport due to aqueous or hydrothermal processes. Three of the elements, Li, Be, and B, have higher concentrations in the upper suevite impact breccias than in the lower impact melt deposits by factors of 3.5, 2.2, and 1.5, respectively. Lithium and B are the most enriched elements up section, and appear to have had the greatest mobility. The similar fractionation of Li and B is consistent with fluid transport and alteration under low-temperature conditions of less than 150 °C based on published experimental studies. In contrast to Li, Be, and B, the concentration of Ba in the altered matrix materials decreases upward in the section, and the concentration of Ba in the matrix is an order of magnitude less than the bulk concentrations, likely due to the presence of barite. The origin of the elemental variations with depth may be related to different protolith compositions in the upper versus the lower impactite units. A different protolith in the altered matrix is suggested by the Mg-rich composition of the lower units versus the Al-rich composition of the upper units, which largely correlates with the mobile element variations. The possibility that vertical transport of mobile elements is due to a postimpact hydrothermal system is supported by published data showing that the sediments immediately overlying the impactites are enriched in mobile elements derived from a hydrothermal system. However, the mobile elements in the sediments do not have to originate from the underlying impactites. In conclusion, our data suggests that the impactites at this location did not experience extensive high-temperature hydrothermal processing, and that only limited transport of some elements, including Li, Be, and B, occurred.

INTRODUCTION

Hydrothermal processes have been documented in many large terrestrial impact structures such as the Sudbury structure, the Ries crater, the Manson structure, and craters in Russia (e.g., Newsom et al. 1986; Ames et al. 1998; McCarville and Crossey 1996; Naumov 2002). Aqueous and hydrothermal processes in Martian impact craters may have contributed to the mobile element content of the Martian soil (e.g., Newsom and Hagerty 1997; Newsom et al. 1999; 2001; Bullock et al. 2004) and possibly to the rock component of the soil (Nelson et al. 2005). Hydrothermal alteration in terrestrial craters occurs in association with the impact melt deposits on the crater floor, at the crater rim, in the central uplift, and in the shocked basement adjacent to the crater fill (Newsom et al. 2001; Naumov 2002). For example, the Haughton structure in Canada exhibits chimneys (degassing pipes) mineralized with quartz, sulfide, sulfate, and carbonate minerals, with formation temperatures ranging from less than 100 °C to greater than 200 °C (Osinski et al. 2001; Osinski et al. 2005). Hydrothermal processes have recently been documented in small craters including the Kärdla crater, which is 4 km in diameter (Kirsimae et al. 2002; Puura et al. 2004), based on chloritization and the presence of secondary quartz containing fluid inclusions formed at 150–300 °C. The Lonar crater, which is 1.8 km in diameter, is about the smallest crater to have evidence of limited postimpact hydrothermal alteration, which is found in basement rocks beneath the crater floor (Hagerty and Newsom 2003).

The Chicxulub impact structure in the Yucatán Peninsula is one of the largest impact craters identified so far on the Earth, with a diameter of 180–200 km, and is associated with

the mass extinction at the K/T boundary (e.g., Alvarez et al. 1980; Hildebrand et al. 1991; Pope 2002). An improved understanding of the formation of such large impact craters or basins can provide important insights into the nature and history of the hydrothermal processes associated with large impacts into planetary bodies (Newsom 1980; Brackenridge et al. 1985; Newsom et al. 1986, 2001; Naumov 2002).

The Yaxcopoil-1 drill hole (Yax-1) is located just outside of the transient cavity of the crater, which explains some of the unusual characteristics of the core stratigraphy (Dressler et al. 2003). In particular, the impact melt and breccias are only 100 m thick, which is surprising considering the thicker breccia accumulations encountered by various industrial and scientific drill holes relatively nearby (e.g., Hildebrand et al. 1991; Claeys et al. 2003).

The impact breccias in the Yax-1 drill hole were divided into six units (Dressler et al. 2003, 2004), which we use here. An alternative numbering system by Tuchscherer et al. (2004) combines the Dressler units 1 and 2 into a unit 1, reducing the number of units from six to five. The two uppermost units are redeposited suevite (unit 1, ~13 m thick) and suevite (unit 2, 808.82–822.88 m). The lower four units are interpreted to be a ground surge deposit, with the upper two consisting of relatively fewer large clasts and melt clasts among fine-grained groundmass (unit 3, brown melt-bearing breccia 845.82–861.08 m), and a coarse suevitic breccia (unit 4, 845.82–861.08 m) below. Below unit 4 is melt breccia consisting of green, laminated melt fragments, silicate clasts, and calcite (unit 5, 861.08–884.94 m); the final unit is very Ca-rich, with silicate melt fragments among what may be carbonate melt (unit 6, 10 m thick). We have concentrated our analytical work on the fine-grained groundmass (matrix) between the larger basement clasts in units 2–5.

According to Ames et al. (2004), there are 25 m of basal tertiary carbonate overlying the impactites (770.43–789.61 m). The carbonates contain sulfide-smectite aggregates with elevated contents of Ni, Ag, Au, Bi, and Te in marcasite, and Cd and Ga in sphalerite. Enrichments in other fluid mobile elements have been noted at the base of this sequence by Rowe et al. (2004). The enrichments could be due to hydrothermal upwelling from a mafic source (Rowe et al. 2004; Ames et al. 2004).

Initial studies of the mineralogy and geochemistry of the impactites in the drill core identified the presence of alteration phases due to postimpact hydrothermal processes (Tuchscherer et al. 2004, 2005; Hecht et al. 2004; Ames et al. 2004; Zürcher and Kring 2004). Variations in the concentrations of mobile elements in the core have been documented with bulk analyses of the impactite breccias by Tuchscherer et al. (2004, 2005), and by bulk analyses of the carbonate-rich sediments overlying the impact breccias by Rowe et al. (2004). We have analyzed altered and hydrated material having the textural characteristics of clays in thin section with electron microprobe, SIMS, and X-ray diffraction (XRD) to see if there is trace element evidence for fluid mobile element transport. These alteration phases are in the matrix or groundmass in units 3 and 4, but also include altered clasts in the upper units 2 and 3.

ANALYTICAL APPROACH

Electron Microprobe (EMP) and X-ray Diffraction (XRD)

Prior to trace element analysis, individual phases in the Yaxcopoil thin sections were imaged and analyzed for major elements using the JEOL 8200 electron microprobe and the JEOL 5800LV SEM in the Institute of Meteoritics of the University of New Mexico. The JEOL 8200 uses a LaB6 electron gun, and five wavelength-dispersive (WD) spectrometers. Quantitative analyses were obtained with a 15 KeV accelerating voltage and 20 nA sample current, and using ZAF correction routines. The mineral calibration standards were orthoclase (Al_2O_3, SiO_2, K_2O), albite (NaO), diopside (MgO, Ca) and olivine (FeO).

X-ray diffraction studies of separated clay minerals from the core samples were also conducted to determine the mineralogical nature of the clays. The visible matrix between target rock clasts was extracted using a drill, larger grains were sifted out, and further clay separation was done with a centrifuge (Moore and Reynolds 1997). Clay slurries were then prepared for analysis in a Scintag PadV XRD, over the 2θ range from 2 to 35 or 40 degrees, with 0.05 degree step intervals, and a dwell time of 4 s. Automatic background removal was done for the profiles. The main 2σ peak data, in degrees, for the samples are as follows: from Yax-1 647 unit 4–6.9° air, 5.35° glycolated, Yax-1 647 unit 4–7.6° air, 7.05° glycolated, 9.1° baked, from Yax-1 628 unit 2–7.1° air, 6.85° glycolated, and Yax-1 641 unit 5–6.45° air, 6.65° glycolated.

Secondary Ion Mass Spectrometry (SIMS)

The SIMS technique has been routinely used in recent years for the determination of the abundances of Li, Be, B, and Ba in common igneous minerals (e.g., Herd et al. 2002, 2004; Hervig 2002; Lentz et al. 2000, 2001), and some pegmatite phases like tourmaline (e.g., Grew et al. 1997, 1998a, 1998b, 1998c, 2003). Hawthorne et al. (1995) reported, for example, that "calibration curves using this technique for Li/Si, Be/Si, and B/Si hold over extended ranges of concentration from ppm to weight percent for light elements in matrices with silica contents ranging from 20% to 80% SiO_2." However, analyses of hydrous minerals and clay minerals by SIMS are scarce. Bridges and Grady (1999, 2000), for example, analyzed the abundance of Ba in the Lafayette Martian meteorite. To better validate the technique for alteration minerals, we analyzed a range of samples from hydrous clays to glass standards to examine the potential matrix effects and the linearity of the instrument response for

Table 1. Geochemical reference standards and secondary calibration materials (analyzed by other methods) used in this study. Data are limited to three significant figures to avoid rounding errors, except for the geochemical reference standards NIST 610 and NIST 612.

Name and abbreviations	Type of material	References	B (ppm)	Ba (ppm)	Be (ppm)	Li (ppm)	SiO_2 (wt%)	FeO (wt%)	MnO (wt%)
NIST 610	Synthetic glass	Ba (a) Li, Be, B (b)	356.4	430.7	465.6	484.6	70	0.056	0.054
NIST 612	Synthetic glass	b	34.73	37.74	37.73	41.54	71.9	0.02	0.01
PRS 1940, Prismatine BM 1940	Prismatine 1	c	12,000	–	79.2	883.0	29.5	11.93	0.12
Bio 8, Biotite 5-9/20/1961	Biotite	d, e	11.1	–	–	160	35.0	20.4	0.13
Bio 9, Biotite 16-7/18/1960	Biotite	d, e	17.1	–	–	69.4	34.4	19.3	0.16
Biora, Biotite RA-A31-66	Biotite	d	–	–	–	2380	35.6	21.6	0.42
9-8763	Muscovite	d	–	–	–	102	45.6	1	–
OK-27	Muscovite	d	–	–	–	652	46.8	1.78	0.03
Sill 556, Sillimanite 556	Sillimanite	d, e	19.1	–	–	–	36.6	2.01	–
Sill-K, Sillimanite Kerrick's	Sillimanite	d, e	200	–	–	–	36.4	0.4	–
Elbaite, Tourmaline 98144	Tourmaline, Elbaite	f	30,100	–	–	4580	36.5	6.3	0.2
PRS112, Prismatine 112233	Tourmaline, Prismatine	f	11,200	–	–	–	31.7	1.54	0.02
Schorl, Tourmaline 112566	Tourmaline, Lithian schorl	f	31,800	–	–	416	33.3	13.8	1.2
1950, MU 1950 Biotite	Biotite	g	–	1964	–	438	38.8	13.9	–
Bio1, Hull 1959 biotite	Biotite	g	–	635	–	661	35.0	25.1	0.69
GP, Glacier Peak biotite	Biotite	g	–	1055	–	836	35.0	25.0	0.79
HDM0	Rhyolite glass	h	10.9	27	3.9	41.6	76.6	0.79	–
JDFD2	Basaltic glass	i	–	–	0.63	7.80	50.1	12.2	0.22
AII93, AII93-11-103	Basaltic glass	j	–	7.8	–	–	51.8	8.75	0.167

References: a = data from Rocholl et al. (2000); b = data from Pearce et al. (1997); c = data from Grew et al. (1990); d = data from E. S. Grew, personal communication (1998); e = data from Paul (2005); f = data from Dyar et al. (2001); g = data from A. Brearley, personal communication (2001); h = data from G. Layne, personal communication (1994); i = data from Wallace and Carmichael (1992); j = data from Newsom et al. (1986).

this application. A large set of samples with trace element abundances measured by other methods (e.g., Grew et al. 1998a, 1998b, 1998c, 2003) were analyzed by SIMS including the NIST 610 and NIST 612 geochemical reference standards, which cover a large range of abundances of Li, Be, B, and Ba (Table 1). Other samples were specifically included to investigate the potential for matrix effects due to iron and manganese.

Analyses were performed with a Cameca IMS 4-f ion microprobe (Institute of Meteoritics, University of New Mexico) using primary O^- ions accelerated through a nominal potential of 10 kV. A primary beam current of 10 nA is focused on the sample over a spot diameter of 8 to 10 μm. Sputtered secondary ions are energy filtered using an offset of 105 V and an energy window of 50 V (e.g., Grew et al. 1998a, 1998b). A typical spot analysis consists of 20 counting cycles, with individual peak-counting times for $^7Li^+$ (2 s), $^9Be^+$ (5 s), $^{11}B^+$ (3 s), $^{30}Si^+$ (2 s), and background at a mass of 6.5 (2 s). The area to be analyzed is first sputtered in raster mode for 3 min to clean off any residual surface contamination, especially boron. After switching to a stationary beam, the magnet is cycled through the mass sequence before the initial data accumulation cycle is started. Even with these precautions the resulting counts for each element in each counting cycle are examined, as occasionally surface contamination, such as boron, can be present in a few of the early cycles. Analyses where the data continuously vary throughout the collection period are rejected. Absolute concentrations of each element are calculated for unknown sample concentrations relative to the NIST 610 geochemical reference standard (see justification below) using the relationship of the intensity of the peak for the element of interest, normalized to the intensity of the peak for Si multiplied by the known SiO_2 content in wt% (only silicates were analyzed in this study). The formula used in the calculations (Shimizu and Hart 1982) using lithium as an example is as follows:

$Li_{unknown}$ ppm = $[(^7Li_{unknown}/^{30}Si_{unknown}) * SiO_{2\ unknown}] * (Li_{std}$ ppm / $[(^7Li_{std}/^{30}Si_{std}) * SiO_{2\ std}])$, where $Li_{unknown}$ is the concentration of Li in the unknown sample, and std is a standard (NIST 610 for this study).

The standardization process for the ion probe involves determining the relationship between the concentration of the element of interest in the unknown and the intensity of the signal for the appropriate mass. This function is generally determined from a linear best fit to several standards, or from a single standard with the assumption that the calibration curve passes through the zero intensity and zero concentration

Table 2. Results from SIMS analysis of standards and calibration materials for Li, Be, B, Ba, and Si (for normalization). The reported values refer to the silicon normalized ratios (SNR) for the intensities of the trace element and silicon in the form of $[(\text{Element/Si})_{\text{SIMS intensity ratio}}*\text{Concentration } SiO_2{}^{\text{standard}}]/\text{Concentration Element}^{\text{standard}}$, as explained in the text.

Element	Lithium All stds.	Lithium 610 only	Beryllium All stds.	Beryllium 610 only	Boron All stds.	Boron 610 only	Barium All stds.	Barium 610 only
Number of analyses	41	10	26	10	33	11	30	10
SNR: Mean	4.05E-02	3.95E-02	1.03E-01	9.71E-02	9.95E-03	9.11E-03	1.45E-03	1.46E-03
SNR: Standard dev.	5.56E-03	2.19E-03	8.28E-03	5.08E-03	2.45E-03	7.82E-04	1.29E-04	8.65E-05
SNR: Percent std. dev.	13.7	5.54	8.05	5.23	24.6	8.59	8.86	5.94
SNR: Population std. dev.	8.68E-04	6.92E-04	1.62E-03	1.60E-03	4.27E-04	2.36E-04	2.35E-05	2.74E-05
SNR: Percent pop. std. dev.	2.14	1.75	1.58	1.65	4.29	2.59	1.62	1.88

point. In order to compare the results for a number of standards whose trace elements have been measured by other techniques, we have calculated the slope of the calibration curve through zero for a wide range of standards. In keeping with other publications from the UNM SIMS laboratory, the Y axis of the data plotted in Figs. 1a–d and Fig. 2 is $[(El_{std}/{}^{30}Si_{std}) * SiO_{2\ std}])/El_{std}$ ppm, which is the slope of the calibration line through the origin on a plot of SiO_2 normalized intensity ratios versus element concentration.

The results clearly show that the slope factors for each known sample are reproducible and independent of concentrations (Table 2; Figs. 1a–d). For example, the measurements of the average slope factor for the NIST 610 standard (Table 2) have a population standard deviation of 2% for Li, Be, and Ba, and less than 3% for B, for analyses over a five-year period. This small analytical precision permits comparison of analyses done at different times.

The linear response of the instrument as a function of concentration is indicated by the relatively small uncertainty of the data for the known samples (Figs. 1a–d; Table 2). The slope factor data show no systemic differences as a function of concentration down to less than 10 ppm for Li, Ba, and B, and down to 4 ppm for Be. The two geochemical reference standards (NIST 610 and NIST 612) fall into the middle of the more scattered results for the natural standard materials. This is to be expected due to the homogeneity of the artificial standards and the large number of analyses of these materials. The analytical accuracy of the technique is represented by the one sigma standard deviation for the different trace elements in the 610 standard (Table 2) of <6% for Li, Be, B, and <9% for Ba. The actual detection limits determined from the counting statistics are 10 ppb for B, Li, and Be, and 100 ppb for Ba.

Based on the reproducibility and linearity of the instrument response, we concluded that the best calibration procedure for each run was to use the NIST 610 standard in each run as the primary standard, with at least one other standard for confirmation of the calibration. This procedure uses the best-characterized standard (NIST 610) and reduces the time spent on analyzing multiple standards in each run. Utilizing the calibration value determined for each run avoids any slight drift of the calibration that can occur over several years. Tying the results to the NIST 610 standard also allows future correction of these results to any minor changes in the accepted abundances of this standard. For example, the Bridges and Grady (1999, 2000) analyses of Ba in the Lafayette Martian meteorite used the NIST 610 glass standard, but assumed a Ba concentration of 351 ppm, whereas the current best value for this standard is 430.7 ppm (Rocholl et al. 2000).

A possible matrix effect for lithium due to different FeO + MnO abundances was discussed by Ottolini and Hawthorne (2001). Ottolini et al. (1993) showed that energy filtering reduces the low-energy ions responsible for matrix effects. Using energy filtering analyses of Fe-rich glass and biotite standards are independent of FeO + MnO concentration. This indicates that no matrix effect is present, given the uncertainties of the trace element abundances in the available materials with known compositions.

An important limitation of the SIMS technique as applied here is the need to determine the SiO_2 abundance of the unknown sample as part of the analytical procedure. In this study, the fine-grained nature and heterogeneity of many of the materials analyzed (reported below) may explain some of the variability of analyses made on the same thin section. In addition, interference from Al^{3+} in aluminum-rich phases could be a significant problem for some of the beryllium analyses.

RESULTS

The samples used for this study represent units 2–5 (808.82–884.94 m) of the impact breccias identified in the drill core (Dressler et al. 2003, 2004). The primary materials analyzed for this study are found associated with the matrix material between larger melt clasts, including altered glass fragments and vesicle and vein fillings. Because of the complexity of the petrography, and to avoid confusion over nomenclature, secondary electron or backscattered electron images (Fig. 3) are presented with the location of every SIMS

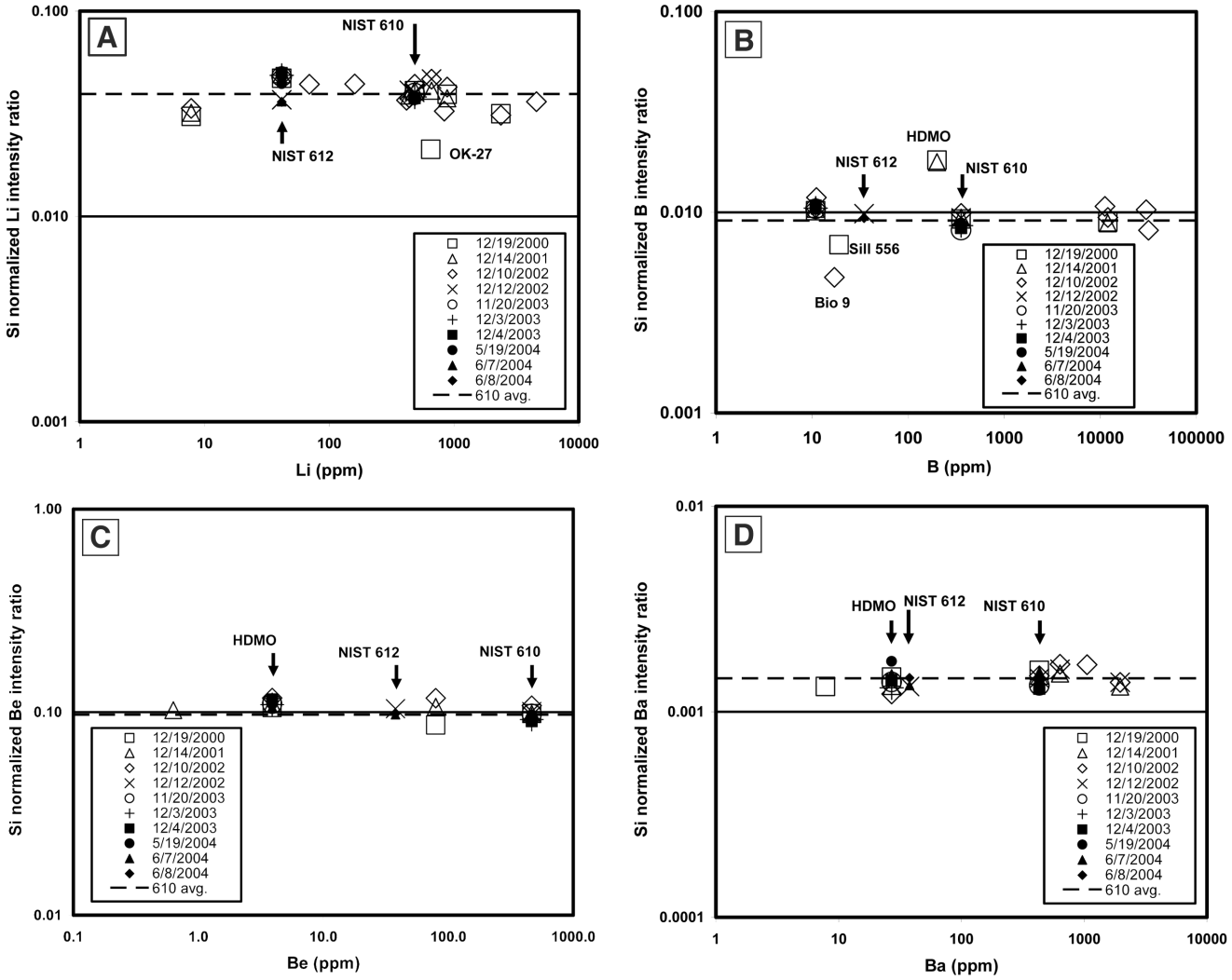

Fig. 1. Si-normalized intensity ratios (see text) for (a) lithium, (b) boron, (c) beryllium, and (d) barium as a function of the concentration of the elements in the standards. The identification of the largest outliers are labeled as in Table 1.

analysis point in this study. The areas selected for analysis usually have what we call a desiccation texture consisting of cracks that appear to represent shrinkage due to dehydration, consistent with the presence of alteration clay minerals. The low totals for the microprobe analyses (Table 3) are consistent with the presence of water, supporting the interpretation that these materials consist of water-bearing phyllosilicate minerals as detected in the X-ray diffraction study of the clay-size separated fraction.

The detailed nature and source stratigraphic units of the samples and thin sections analyzed in this study are as follows:

- Unit 2. Designated as redeposited suevite (Dressler et al. 2004), lower sorted suevite (Stöffler et al. 2004), or reworked suevite (Tuchscherer et al. 2004). In addition to the groundmass, the unit contains many round to angular fragments of vesicle rims. These fragments sometimes exhibit shard-like appearance and clay linings, often with flow texture around them. The material analyzed in sample Yax-1 628 from 809 m depth consisted of a clast of altered glass with a desiccated texture, vesicle linings, and vesicle fillings (Figs. 3a–c).
- Unit 3. Designated as chocolate brown melt breccia (Dressler et al. 2004), upper suevite (Stöffler et al. 2004), or suevite (Tuchscherer et al. 2004). Observations by Nelson and Newsom (2006) suggest that the material in sample Yax-1 634, 837 m depth (Fig. 3d) consists of vesicular clasts and shards that appear to be surrounded by a fine-grained, carbonate-rich vesicular melt. The possible implications of these observations are not considered here, as the materials analyzed in this section do not include the possible melts. The SIMS analyses only included possible glass shards in the matrix, and vesicle fillings with a desiccated texture.

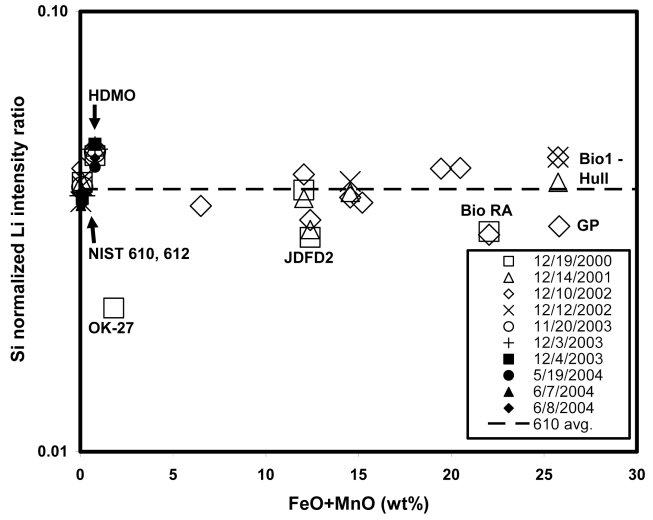

Fig. 2. Silicon normalized lithium intensity ratio (see text) versus FeO + MnO. The absence of a systematic variation in the intensity ratio as a function of FeO + MnO concentration suggests that matrix effects due to Fe or Mn are not significant within a few percent (see text). The largest outliers are labeled (Table 1).

- Unit 4. Designated as variegated glass-rich suevitic breccia (Dressler et al. 2004), middle suevite (Stöffler et al. 2004), or variegated suevite (Tuchscherer et al. 2004). Two samples were studied from this unit, Yax-1 647, 848 m depth, and Yax-1 641, 857 m depth. The material analyzed in this sample consists of a groundmass containing altered vesicular glass shards, surrounded by Fe-poor saponite composition phyllosilicate with desiccation textures (Figs. 3e–h). The material analyzed in sample Yax-1 641 consists of only vesicle fillings with desiccated texture and an altered melt clast.
- Unit 5. Designated as green monomict autogene melt breccia (Dressler et al. 2004), brecciated impact melt rock (Stöffler et al. 2004), and green impact melt breccia (Tuchscherer et al. 2004). This unit is chemically similar to unit 4, but the unit exhibits less schlieren texture than in unit 4, and clasts and fragments are more angular in appearance. The material analyzed in thin section Yax-1 643 from 862 m depth includes clasts of recrystallized melt. The altered matrix analyzed in this section consists of saponite-composition material with desiccation features (Figs. 3i–k).

The trace element results from this study are listed in Table 3, along with major element abundances determined by electron microprobe on the same spots. These microprobe data and X-ray diffraction data are consistent with the presence of smectite, probably montmorillonite, which dominates in units 2 and 3. Mg-saponite dominates in unit 4 and unit 5. Using X-ray diffraction and mineral chemical analyses, Ames et al. (2004) identified the presence of K montmorillonite in Units 1, 2, and the top half of 3, and Mg saponite in the bottom half of unit 3 and below. The swelling behavior of these clays after glycolation is also consistent with smectite. Ames et al. (2004) also occasionally found celadonite, an optically green clay with relatively high FeO content (18–22 wt%), in units 1 and 2, but no clays with this composition are represented in our samples.

The analytical data for the altered matrix material show interesting trends as a function of depth in the drill core (Figs. 4a–c, 5a–c, 6a–b). The concentrations of elements Li, B, and Be generally increase upward along the core, with Li > B > Be, whereas the Ba concentration in the altered matrix materials decreases upward. The abundances of the elements Li and B are well correlated with each other (Fig. 5b) and somewhat correlated with Be (Fig. 5c), with correlation coefficients for Li-B = 0.89, B-Be = 0.71, and Li-Be = 0.50. Ratios between trace element concentrations in the different units are listed in Table 4.

The abundances of the major elements FeO and Al_2O_3 as a function of depth are shown in Fig. 6. The composition of the individual microprobe analyses (Table 3) reflect the compositions of the altered matrix materials. The altered matrix materials in the upper units generally have higher FeO and Al_2O_3 contents than reflected by the bulk analyses of Tuchscherer et al. (2004), with a smectite composition. The lower units have the Mg saponite composition with lower FeO and Al_2O_3 contents than shown in the bulk analyses from Tuchscherer et al. (2004).

In addition to analyzing the altered matrix materials that have a desiccated texture, melt clasts were analyzed to understand the possible protolith for the altered matrix. We have determined the abundances in the melt clasts from unit 5 (Yax-1 643) and from melt in units 3 and 4. Our results favorably compare (Table 5) with those of Ames et al. (2004) and Tuchscherer et al. (2004). The melt clasts have Al_2O_3, and Li, Ba, and Be abundances that are surprisingly similar to the bulk continental crust abundances of Taylor and McLennan (1985). A recently revised Li abundance in the continental crust of 35 ppm (Teng et al. 2004) is higher than the earlier estimate of 13 ppm (Taylor and McLennan 1985). However, boron abundances in the melt clasts are about 5 times higher than the continental crust abundances. A continental crustal composition for the protolith is consistent with the nature of the bedrock at Chicxulub, and the presence of quartz in the distal K/T boundary clay.

Compared to the melt clasts, Li and B in the altered matrix have similar abundances in the lower units 4 and 5, and are enriched in the upper units 2 and 3 (Figs. 4a and 5a). The Be concentrations in the altered matrix range from equal to somewhat lower than the melt clasts in units 4 and 5, to equal and somewhat higher in the upper units 3 and 4 (Figs. 4b and 5c). In contrast, the Ba concentrations in the altered matrix material are lower than the Ba concentrations in the melt clasts and the continental crust (Fig. 4c).

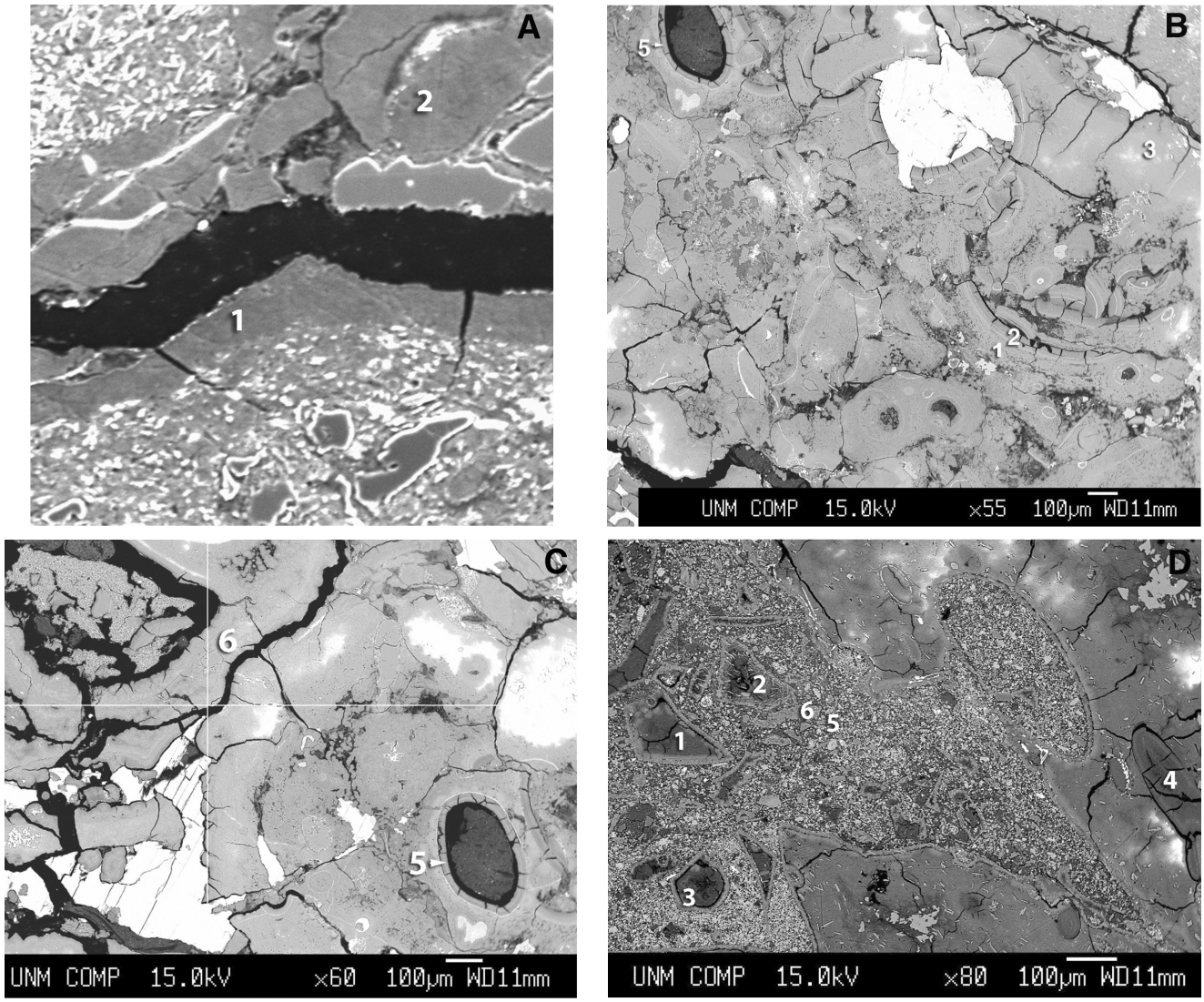

Fig. 3. a) A secondary electron image of a portion of sample Yax-1 628, referred to as area 1, from Unit 2 at 809 m depth. SIMS analyses points 1 and 2 are of the suevite groundmass, with a desiccated texture. Most of the altered material in units 2 and 3 has an Al-rich smectite composition. Image width is approximately 75 µm. b) A backscattered electron image of a portion of Yax-1 628, referred to as area 4 from unit 2 at 809 m depth. SIMS analyses points 1 and 5 are of fragments of vesicle rims that have clay desiccation texture (what Hecht et al. [2004] calls Sm2), while point 2 is a rim-groundmass (matrix) boundary (Hecht et al. [2004] Sm 1). Point 3 is of the suevite groundmass, which has largely been altered to smectite (Hecht et al. 2004 Sm 1). c) A backscattered image of the area adjacent to Fig. 3 of Yax-1 628, area 4 from unit 2. This area consists of vesicular groundmass material, with vesicle fillings and altered rims. Point 6 is part of the suevite groundmass. Several generations of clay mineral formation described by Hecht et al. (2004) are visible. SIMS analysis point 6 is an altered clast (Hecht Sm 1). SIMS point 5 is a vesicle lining (Hecht Sm 2). The vesicle fillings are like Hecht Sm 3. d) A backscattered electron image of suevite sample Yax-1 634, area 8 from unit 3 at 837 m depth, which is typical of the upper samples in our study. The sample consists of vesicular glass shards altered to clays with a saponite composition and desiccated texture among the fine-grained, carbonate-rich matrix.

DISCUSSION

Evidence for Hydrothermal Alteration

Petrographic evidence for hydrothermal alteration has been documented in the Yax-1 impactites by several studies (Ames et al. 2004; Hecht et al. 2004; Lüders and Rickers 2004; Zürcher and Kring 2004; Rowe et al. 2004; Tuchscherer et al. 2004, 2005; Goto et al. 2004). This alteration has been divided into a sequence with several different stages by Zürcher and Kring (2004). Their earliest stage is the metasomatic replacement of pyroxene and plagioclase at a temperature greater than 300 °C. During this stage, primary augite is replaced by secondary diopside, and Na plagioclase replaced primary plagioclase. The widespread occurrence of feldspar with variable substitution of Na and K for Ca is consistent with a combination of replacement and deposition of hydrothermal plagioclase. This could have occurred due to

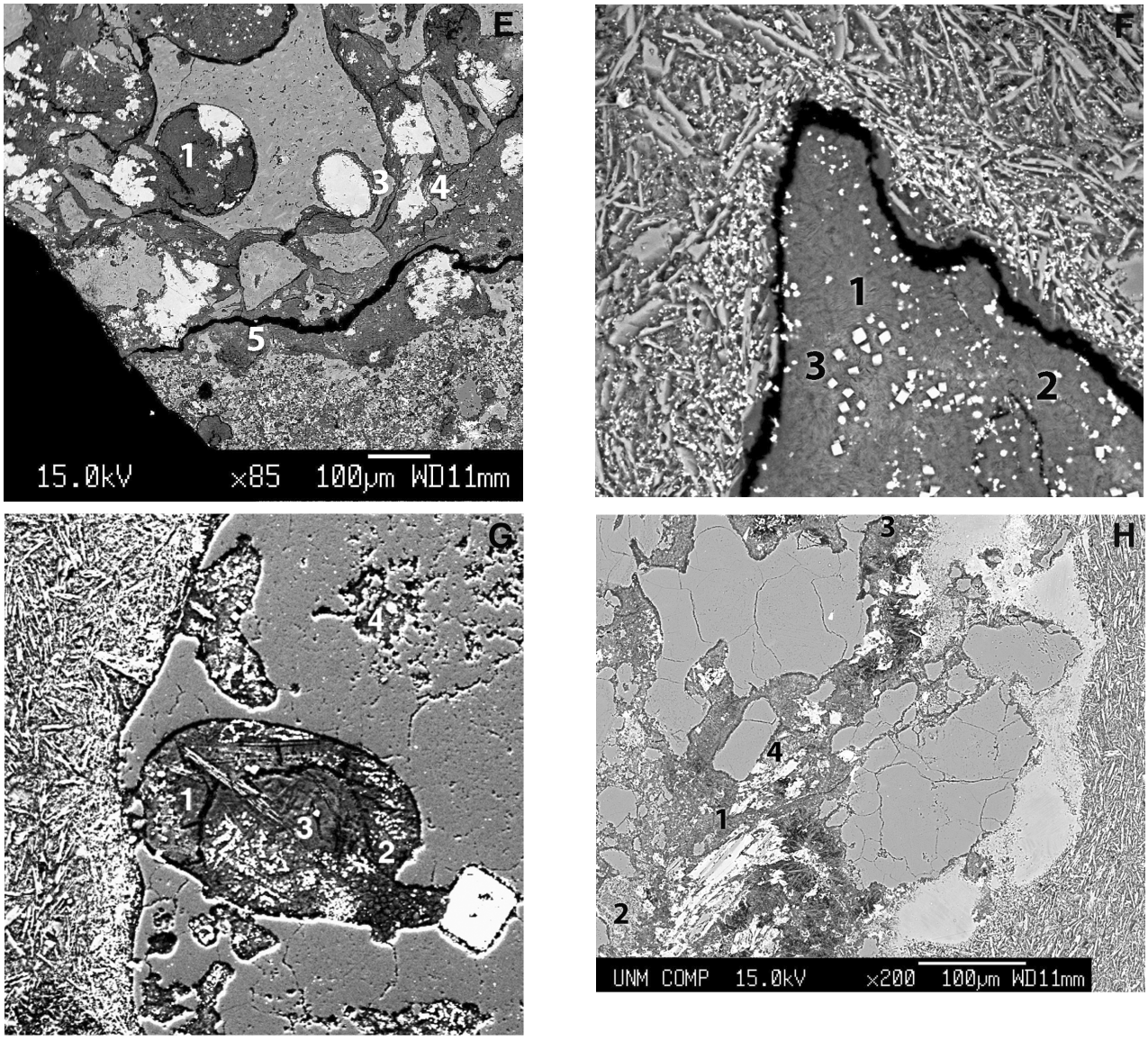

Fig. 3. *Continued.* e) A backscattered electron image of Yax-1 647, area 5 from unit 4 melt breccia at 848 m depth. The sample consists of a matrix containing vesicular glass shards, surrounded by Fe-poor saponite composition clays with desiccation textures. SIMS points 1, 4, and 5 have a saponite composition, and point 3 is a silicate melt clast with a more Al-rich composition. Most of the altered material analyzed in units 4 and 5 has an Mg-rich saponite composition. f) A secondary electron image of Yax-1 641, area 1 from unit 4 melt breccia at 857 m depth. SIMS points 1, 2, and 3 have a saponite composition. Image width is approximately 100 µm. g) A secondary electron image of Yax-1 641 area 2 from unit 4. SIMS points 1, 2, 3, and 4 are analyses of vesicle clay filling. Image width is approximately 100 µm. h) A backscattered image of Yax-1 641, area 3 from unit 4. SIMS point 1 has a saponite composition, and point 2 is likely a recrystallized melt clast.

a reduced fluid together with the deposition of sulfide. This proposed early event, with temperatures >200 °C, is supported by studies of fluid inclusions in quartz crystals in vugs hosted by Cretaceous limestone below the impact breccias (Lüders and Rickers 2004). However, the existence of this early stage of alteration has been disputed by Tuchscherer et al. (2004) and was not recognized by Hecht et al. (2004).

The formation of the altered materials that are the target for the SIMS analyses in this study followed the possible earlier high-temperature phase of alteration. Hecht et al. (2004) related to this stage three generations of secondary mineral formation. First was the alteration of glass to Al-rich Mg-poor smectite in units 2 and 3, which is consistent with our microprobe and X-ray diffraction data. Second was the formation of rims on vesicles in units 2 and 3. The last stage of phyllosilicate formation is represented by vesicle fillings (Mg-rich Al-poor saponite composition). The alteration of the melt clasts and matrix to Mg-rich saponite in the lower units resulted in a volumetrically greater amount of alteration material than in the upper units. Our petrographic observations of the secondary mineral occurrences in the thin

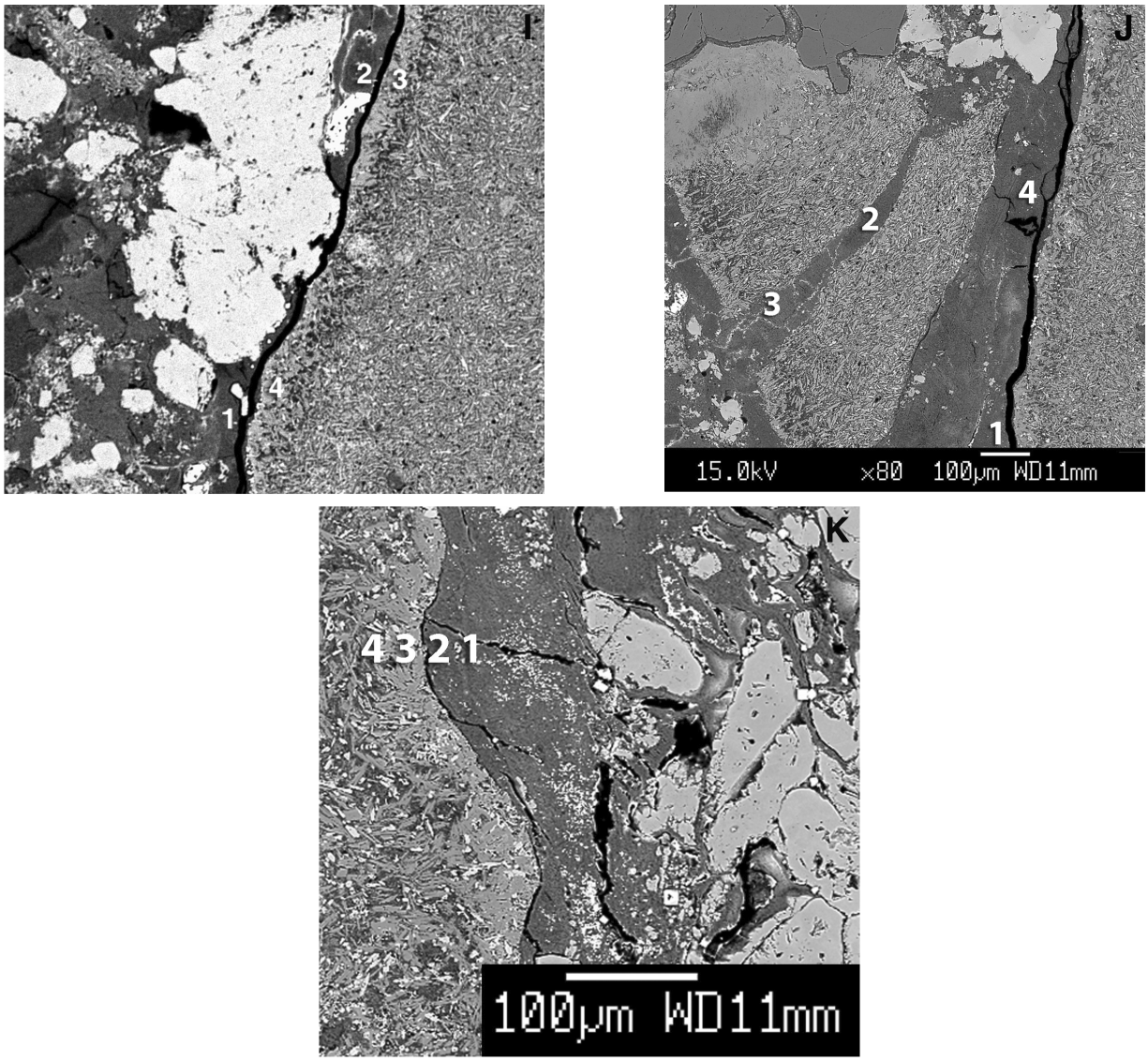

Fig. 3. *Continued.* i) A backscattered electron image of Yax-1 643, area 2 from unit 5 melt breccia at 862 m depth. SIMS analyses points 1 and 2 in the desiccated matrix textured material have a saponite composition; points 3 and 4 are a recrystallized silicate melt clast. Image width is approximately 100 µm. j) A backscattered electron image of Yax-1 643, area 3 from unit 5 at 862 m depth. The section contains clasts of partially recrystallized melt with veins of saponite clay composition material with a desiccated texture. The smaller vein running from lower left to upper right (SIMS points 2 and 3) has higher Ba contents and lower B contents than the large vein filling in the center (SIMS points 1 and 4). k) A backscattered electron image of Yax-1 643, area 4 from unit 5. SIMS analyses points 1 and 2 have a saponite composition, and 3 and 4 are of a recrystallized silicate glass.

sections are generally in agreement with the observations by Hecht et al. (2004). However, there are no obvious differences in the trace element compositions of the different types of secondary minerals, which could be linked to the different stages of alteration as recognized by Hecht et al. (2004). This could be due to equilibration of the altered matrix materials with the last fluid, or else the fluids did not change much during a single alteration episode.

Our microprobe data show that the Al_2O_3 contents of the altered matrix in the upper units 2 and 3 are similar to the abundances in the melt rocks (Table 4; Fig. 6b). The low Al_2O_3 abundances in the matrix of the lower units compared to the bulk abundances may be due to dilution with a dolomite component (Nelson and Newsom 2006).

Evidence for Mobile Element Transport and Hydrothermal Processes

The available geochemical data for the impactites and overlying sediments in the Yax-1 core record substantial variations in elemental abundances as a function of depth. These variations, as discussed in more detail below, include enrichments of mobile elements in the sediments immediately above the impactites, and enrichments in the upper suevitic

Table 3. Electron microprobe (EMP) major element oxide data and secondary ion mass spectrometry (SIMS) trace element data (Li, Be, B, and Ba) of altered clasts and secondary clay minerals in thin section. Data are reported to three significant figures to avoid rounding errors. The accuracy of these analyses was estimated by repeat analyses of the NIST 610 standard during the same runs as the analyses reported here, giving is a one sigma standard deviation of <6% for Li, Be, Ba, and <9% for B (Table 2).

	Sample	Analysis	Depth (m)	SiO_2 (wt%)	Al_2O_3 (wt%)	FeO (wt%)	MgO (wt%)	CaO (wt%)	Na_2O (wt%)	K_2O (wt%)	EMP Tot[a] (wt%)	Li (ppm)	Be (ppm)	B (ppm)	Ba (ppm)
Unit 2	Yax 628	28A432S1	809	51.0	12.6	10.9	5.51	0.87	1.08	5.5	87.4	114	3.10	244	2.44
	Yax 628	28A431S2	809	49.1	14.8	5.8	4.71	1.01	0.78	1.6	77.7	125	1.12	164	4.61
	Yax 628	28A434S3	809	53.4	14.0	9.2	6.07	0.78	1.3	4.5	89.3	121	2.71	223	2.06
	Yax 628	28A43S5	809	44.9	13.6	6.0	3.94	0.73	0.51	2.4	72.1	113	1.08	144	14.9
	Yax 628	28A415S6	809	53.2	14.2	7.9	6.23	0.71	1.98	4.0	88.1	132	2.23	199	2.07
	Yax 628	28A14S1	809	53.3	16.6	5.0	5.60	0.85	2.14	2.0	85.4	137	2.03	206	5.61
	Yax 628	28A16S2	809	51.5	11.9	12.0	5.25	0.67	1.89	3.9	87.1	124	1.41	129	7.87
Unit 3	Yax 634	Y634A8-1	837	53.9	17.6	2.7	5.70	0.73	2.10	1.1	83.7	153	1.86	224	5.51
	Yax 634	Y634A8-2	837	57.4	18.2	3.1	6.46	0.55	2.65	1.5	89.8	81.6	1.80	131	264
	Yax 634	Y634A8-3	837	47.3	15.8	2.5	4.80	0.60	1.50	1.1	73.6	124	1.21	156	2.28
	Yax 634	Y634A8-4	837	53.4	17.6	3.7	5.55	0.88	1.56	2.0	84.6	130	2.20	252	4.17
	Yax 634	Y634A8-5	837	49.8	5.4	2.8	20.8	1.1	1.65	0.22	81.8	79.0	0.896	121	126
	Yax 634	Y634A8-6	837	62.1	18.5	1.0	2.22	1.6	4.30	7.0	96.8	90.5	1.45	148	305
Unit 4	Yax 647	Y647A5-1	848	40.4	9.4	4.6	13.3	1.4	1.43	0.68	71.1	71.0	0.637	79.7	8.95
	Yax 647	Y647A5-3	848	58.3	16.1	0.57	0.114	1.3	4.91	3.4	84.6	26.3	1.53	67.3	376
	Yax 647	Y647A5-4	848	42.9	7.7	5.4	20.8	0.91	3.02	0.31	81.0	85.7	1.18	109	12.6
	Yax 647	Y647A5-5	848	44.2	10.9	4.3	11.9	2.6	1.00	1.3	76.2	27.1	0.909	56.2	68.3
	Yax 641	641A23S1	857	42.4	8.4	5.7	16.6	1.5	1.2	0.90	76.6	38.5	1.80	117	85.9
	Yax 641	641A27S2	857	41.4	7.4	5.7	17.0	1.4	4.2	0.92	78.0	37.5	1.89	123	16.29
	Yax 641	641A21S3	857	40.9	8.5	5.8	14.7	1.6	1.4	1.3	74.2	32.2	1.55	109	62.24
	Yax 641	64A214S4	857	40.7	6.2	7.5	19.4	1.7	3.7	0.28	79.4	28.9	0.103	16.2	4.43
	Yax 641	641A19S1	857	41.8	9.9	5.7	9.85	1.2	0.80	2.5	71.7	25.5	0.697	60.1	50.4
	Yax 641	641A14S2	857	42.4	6.1	5.8	19.3	1.6	1.6	0.007	76.76	28.9	1.11	85.2	17.7
	Yax 641	64A120S3	857	41.0	5.6	5.9	19.5	1.6	1.6	0.001	75.1	21.9	0.431	41.9	34.6
	Yax 641	64A36S1	857	35.5	6.1	9.1	15.5	1.4	2.9	0.41	71.0	13.2	0.483	36.6	34.5
	Yax 641	64A38S2	857	56.4	17.5	0.3	0.21	1.2	4.6	6.0	86.3	15.7	0.722	61.0	131
	Yax 641	64A313S3	857	34.9	10.2	6.7	16.9	0.97	1.1	1.0	71.7	12.8	0.828	41.9	114
	Yax 641	64A310S4	857	52.8	14.2	3.3	5.1	1.3	2.4	5.3	84.4	21.1	0.819	62.1	93.6
Unit 5	Yax 643	643A3151	862	39.5	9.6	6.5	17.2	1.1	0.63	0.80	75.4	54.0	1.76	138	3.66
	Yax 643	643A3102	862	44.0	6.1	5.8	22.0	0.52	2.2	–	80.6	14.5	1.54	41.7	427
	Yax 643	643A3113	862	47.3	6.9	6.6	23.6	0.49	2.8	–	87.7	14.9	1.71	52.2	478
	Yax 643	643A384	862	41.6	8.5	5.3	15.9	1.5	1.1	1.1	75.0	30.8	0.918	97.1	4.90
	Yax 643	643A221	862	45.0	6.5	5.5	20.8	1.3	0.90	–	79.9	17.9	0.069	25.1	3.77
	Yax 643	643A2152	862	41.4	9.0	5.8	18.8	1.3	0.44	0.40	77.1	13.6	1.450	39.2	402
	Yax 643	643A4LS1	862	45.0	6.7	6.2	22.3	1.2	1.7	–	83.1	53.8	1.55	109	16.0
	Yax 643	643A4LS2	862	45.1	8.5	5.3	19.1	1.2	1.7	0.78	81.5	58.8	1.76	114	7.55
	Yax 643	643A4115	862	45.8	8.0	5.4	18.7	1.8	1.2	0.44	81.2	62.0	1.09	164	34.5
Melt	Yax 643	643A4LS3	862	50.1	16.6	4.0	1.49	4.6	4.4	4.8	85.8	62.8	1.79	133	107
	Yax 643	643A4LS4	862	50.4	14.6	2.1	0.74	6.9	4.0	6.4	85.1	16.4	1.75	47.4	485
	Yax 643	643A2163	862	55.1	13.2	5.4	5.3	11.6	3.2	34	97.1	11.9	1.62	52.1	408
	Yax 643	643A274	862	42.8	11.8	3.8	5.0	9.2	3.5	2.4	78.5	6.98	1.12	28.6	332
	Yax 643	Average		49.6	14.1	3.82	3.11	8.07	3.74	4.3	86.6	24.5	1.57	65.3	333

[a]The electron microprobe (EMP) totals for the altered materials in this study do not include water.

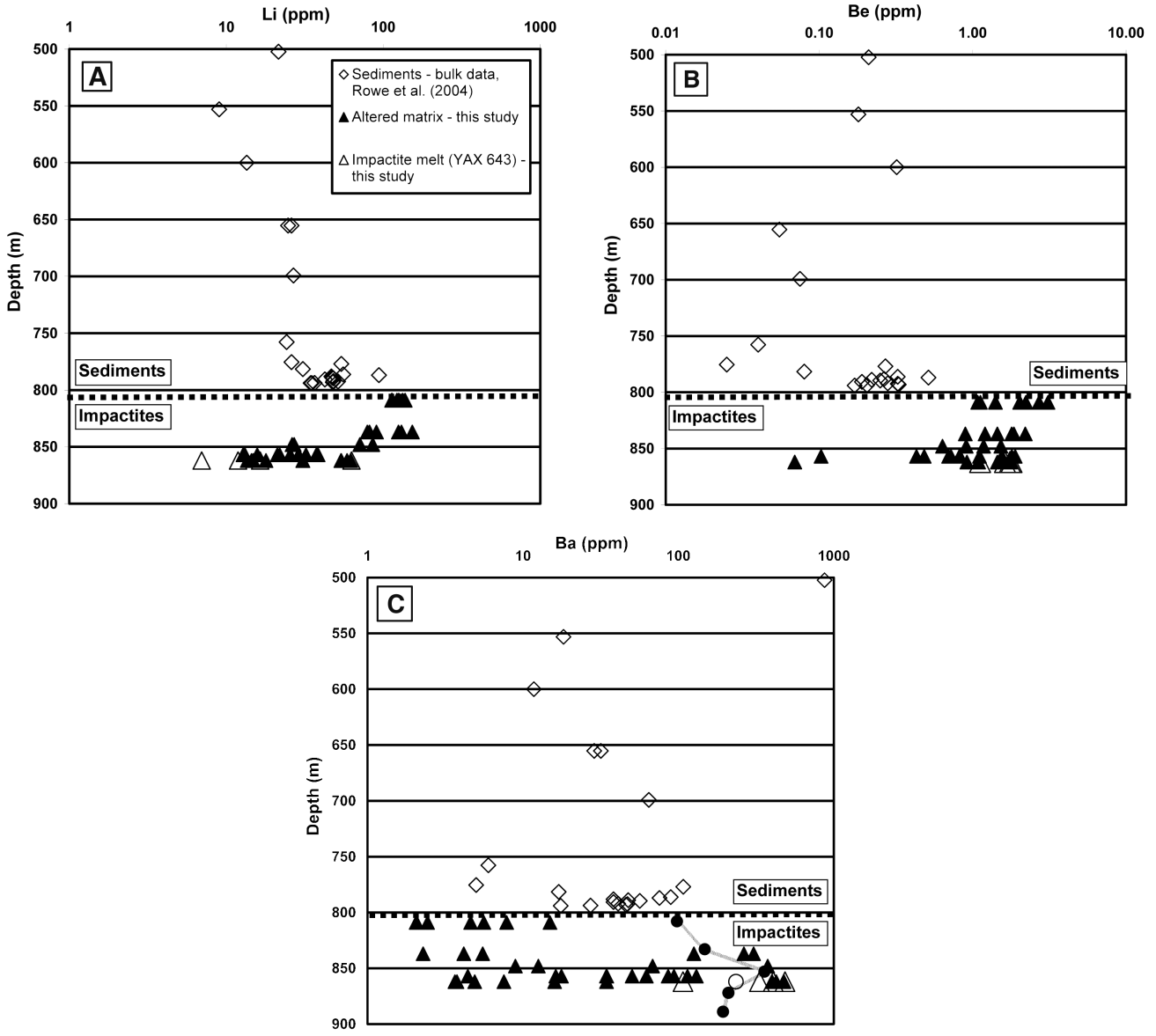

Fig. 4 (a–c) SIMS results for Li, Be, and Ba contents as a function of depth in thin section samples analyzed in this study (Table 1) and in bulk samples analyzed by Rowe et al. (2004) using ICP-AES. The "sediments" analyzed by Rowe et al. (2004) consist of carbonate-rich biomicrites. The "impactite clay" represent materials with alteration textures from units 2–4 analyzed in this study (Table 1). The "impactite melt" are samples of the breccia clasts analyzed in this study (Table 1).

impact units compared to the lower more melt-rich units. In addition to understanding the magnitude of element transport, information about the temperature of the hydrothermal system can be obtained from the relative fractionation of elements such as Li and B. There are several possible explanations for the geochemical variations:

1. Variations in the protolith contributions to the matrix material for each unit may be responsible for the high abundances of Li, Be, and B in the upper impactite units. Tuchscherer et al. (2004) documented an increase in calcium with depth, consistent with the greater proportion of limestone and dolostones. Nelson and Newsom (2006) show evidence for the presence of a dolomitic melt into the lower units, explaining the Mg-rich nature of their matrix. Perhaps the lower abundances of Li, Be, and B in this material could explain the contrast with the suevite units, instead of a difference in precursor materials.
2. Could vertical transport of mobile elements due to upwelling of hydrothermal fluids produce enrichments in the upper units? In the upwelling model, the fluids could have depleted the lower impact breccias in Li, B, and Be and enriched the uppermost impact breccias (seen in both bulk data and the SIMS analyses), and

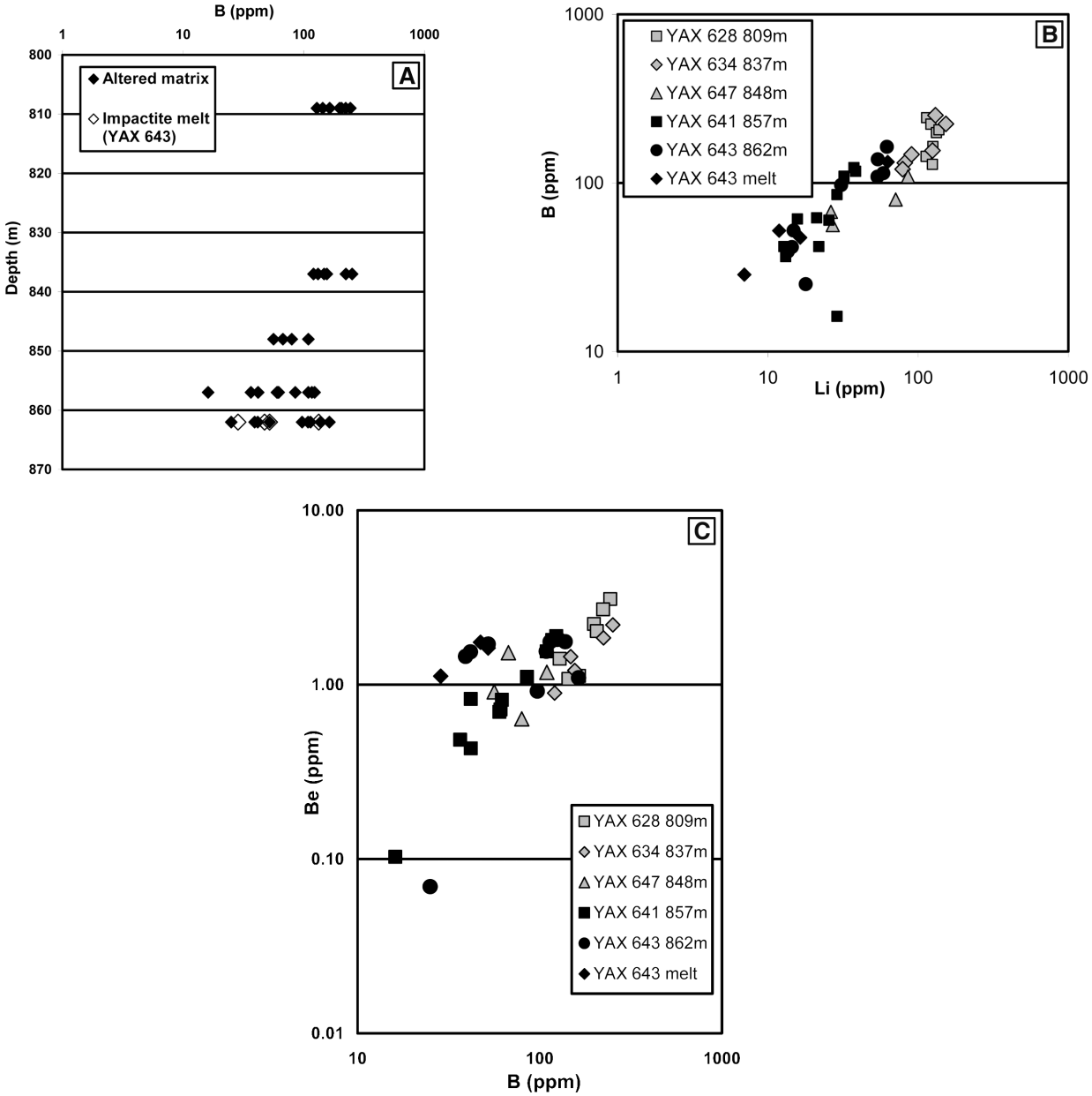

Fig. 5. SIMS data on materials in thin sections from units 2–5 illustrate the behavior of boron concentrations in the core. a) The concentration of B as a function of depth in the impactite. b) The correlation between Li and B concentrations in the impactites. c) The possible correlation between concentration data for Be and B in the impactites.

released fluids containing mobile elements that were incorporated into the sediments overlying the impact breccias (Rowe et al. 2004). There is some limited evidence that fluids rather than protolith variations were responsible for the Li, B, and Be in the alteration phases. The lower suevite Unit 3 and upper impact melt Unit 4 contain both Mg-rich and Mg-poor compositions and Al-rich and Al-poor compositions. However, the trace element abundances in each unit are relatively homogeneous, arguing against the strict control by protolith composition.

3. The unexpectedly thin impactite deposits at the Yax-1 site suggest the possibility that this sector of the ejecta cooled off more quickly, leading to down welling of seawater during the late stages of cooling and alteration, as opposed to upward flow of hydrothermal fluids. In this view, the higher values of the elements in the upper units could reflect the scavenging of the mobile elements from the fluid by the alteration material in the upper units. The lower units would receive water with lower concentrations of the mobile elements (except Ba).

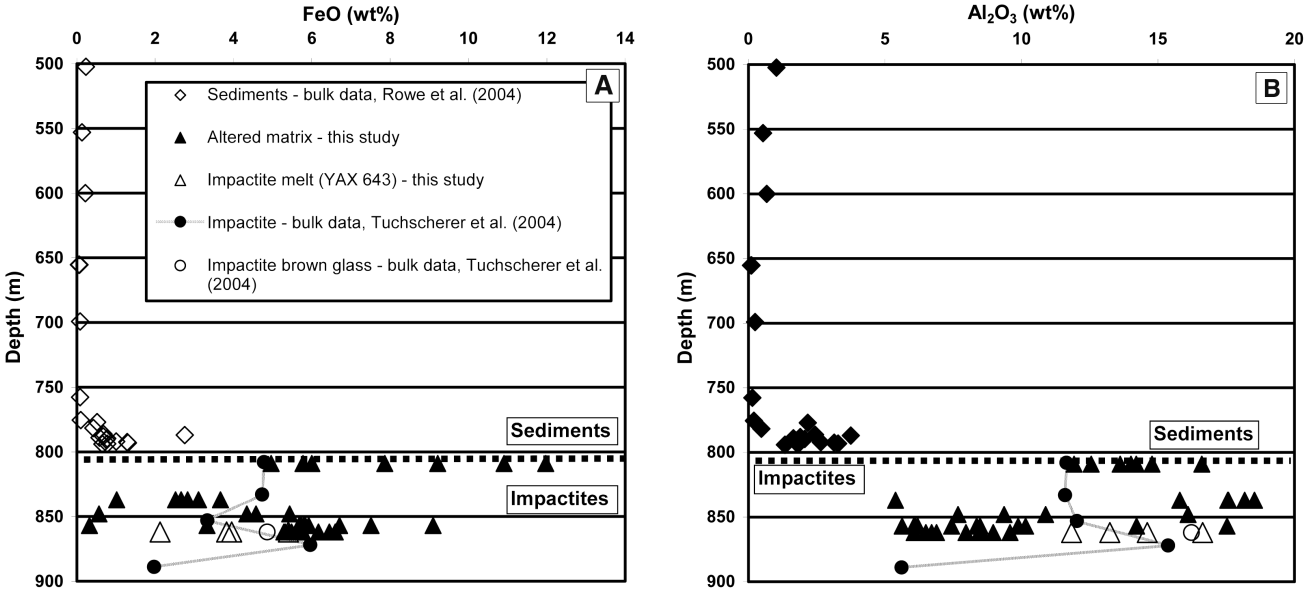

Fig. 6. Major element data for (a) FeO and (b) Al_2O_3 are shown as a function of depth for the impactites and sediments in the Yax-1 core. Data for the altered matrix and impact melt in thin sections from this study were obtained by the electron microprobe for the same locations analyzed by SIMS (Table 1). Bulk data for the sediments above the impactites are from Rowe et al. (2004), while bulk data for the impactites and brown glass are from Tuchscherer et al. (2004).

We will discuss the variations in the trace element abundances at the Yaxcopoil-1 core site in terms of these possibilities.

Mobile Elements in Overlying Sediments

Rowe et al. (2004) presented evidence for hydrothermal transport and deposition of mobile elements in the sediments overlying the impact breccias. Rowe et al. (2004) found that samples of Tertiary biomicrites (consisting of 5–20% bioclasts, and 2% lithoclasts supported by a matrix of carbonate mud) from depths of 794.01 to 777.02 m have higher concentrations of Mn, Fe, P, Ti, Al, Li, and Be relative to samples from higher up in the sediments. They attributed the observed enrichments to elements mobilized by hydrothermal systems in the impact deposits and deposited in the overlying sediments, analogous to hydrothermal deposits in mid-ocean ridge environments. At the Ries crater in Germany, a similar enrichment of mobile elements may be present in the flysch-type graded sandstones and breccias derived from reworked suevite deposited in water in a playa lake environment just above the suevite deposits (Förstner 1977).

One way to look at the possible transport of different elements into the sediments in the Yax-1 core is to apply a mass balance calculation to compare the total mass of an element in the sediments to the amounts in the impactites (Table 5). Using the bulk data from Rowe et al. (2004) and Tuchscherer et al. (2004), the excess Zn, Ba, and FeO in the lower sediments is a small fraction (1.1%, 2.4%, and 4.7%, respectively) of the total in the impact breccias. Similarly, assuming that our abundances in the matrix are representative of the bulk impactites, the extra Li in the sediments above the impact breccias represents less than 7.5%, and Be less than 2.2% of the remaining Li and Be in the altered matrix materials in the impact breccias (units 2–5). Therefore, either the sediments contain only a small amount of the mobilized elements, or the actual amount deposited above the impactites at the Yax-1 site was relatively small.

The sediment data (Rowe et al. 2004) shows an increase in Al_2O_3 just above the impact breccias at the impactite-sediment contact by a factor of 10 compared to higher up in the sediments (Fig. 6b). As aluminum is normally considered an immobile element, the mechanism for the Al_2O_3 enrichment above the contact may involve transport of Al_2O_3-rich clay particles. Rowe et al. (2004) also found an enrichment of FeO by a factor of ten in the sediments directly above the impact breccias, compared to sediments higher up in the stratigraphic section (Fig. 6a), consistent with a higher fraction of silicastic material in the lower sediments. The altered matrix in the upper units has a higher Al_2O_3 content than the bulk rock; therefore, transport of a very small fraction of the alteration phase in the impactite out of the impactites could explain the enrichment in the sediments.

The sediment data of Rowe et al. (2004) support the existence of hydrothermal transport of mobile elements, but the amounts imply only minor transfer to the sediments, or a different source region not connected with the impactites lower in the core. The elements in the sediments could have come from hydrothermal vents in an area with thicker melt deposits and larger heat sources either locally or, less likely, from a more distant source.

Mobile Elements in Impactites

The SIMS data for Li, B, and Be in the altered matrix in the impactites argue for at least local hydrothermal transport at low temperatures. The data of Rowe et al. (2004) for Li and Be, which show enrichments in the sediments directly above the impact breccias (Figs. 6a and 6b), is consistent with hydrothermal mobilization of these elements. However, the different major element composition of the altered matrix material in the upper impactite suggests that a different protolith may have contributed to the upper units.

Possible evidence for upward transport of mobile elements is the enrichment of the altered matrix material in the upper impactite layers in Li, B and Be (and other elements) compared to the lower units. The bulk data of Tuchscherer et al. (2004) for Cs, Au, Rb, and Zn show a similar pattern of enrichment upward in the impactites as the SIMS data for Li, B, and Be in the altered matrix materials (Table 5). For example, Tuchscherer et al. (2004) documented upward enrichments (Table 4) in the concentration of the trace elements in the relative order Cs > Au > Rb = Zn in stratigraphic units 1 to 4. (Note an apparent typo in Tuchscherer et al. 2004. In Table 3, the average Zn in unit 2 should be 55 ppm, not 570 ppm.) The greatest upward increase in the bulk data set is for the abundance of Cs, which increases by a factor of up to 3.7 relative to the lower units, similar to the SIMS data for Li.

FeO can also be mobilized by hydrothermal systems, and is one of the major elements that exhibit upward enrichment in the impactites. Our microprobe data for the points used for SIMS analysis of the altered matrix material shows an enrichment of FeO in unit 2 relative to unit 3 by a factor of 3 (Fig. 6a; Table 4). The bulk data of Tuchscherer et al. (2004) also show some upward enrichment, as the FeO bulk data for units 1 and 2 are higher than that of unit 3.

In contrast to the elements enriched upward in the section, the bulk data show a decrease in the abundance of U, Ba, Na, and K upward in the units, whereas the Ca abundances are highly variable (Tuchscherer et al. 2004). The behavior of Ba in the impact breccias and altered matrix is different from the other mobile elements (Table 4; Fig. 4c). Barium concentrations are higher in the sediments just above the impact breccias suggesting transport due to hydrothermal fluids. However, in both the bulk data for Ba, and the SIMS data for the altered matrix materials in the impactites, there is a substantial decrease in Ba concentrations from the lower to the upper units, opposite to the other mobile elements. The SIMS data for the matrix material shows only a very slight decrease in Ba by a factor of 0.04–0.06 between the suevite of Unit 2 and lower units. The bulk analyses by Tuchscherer et al. (2004) for Ba shows a depletion by a factor of 0.4–0.8 between the suevite of unit 2 and lower units. However, the concentration of Ba in the altered matrix materials determined by SIMS is much lower than the bulk abundance of Ba in the impact breccias at any level by a factor of 0.04 in unit 2 to 0.8 in Unit 5. A complicating factor for Ba is the presence of barite throughout the impactite section, which could help explain the difference between the bulk data and the SIMS data on the altered matrix materials (e.g., Zürcher and Kring 2004). The possibility that the higher bulk Ba content of the lower impact breccias is due to the higher abundance of sedimentary clasts is less likely. For example, the higher bulk U, Na_2O, and K_2O contents in the lower breccias is probably due to depletion of these elements in the upper units.

The relative fractionation of Li and B within and between units provides strong evidence that the temperature of the fluids during the alteration and transport episode was relatively low (<150 °C). Experimental studies of Li and B distribution (Seyfried et al. 1984; Brenan et al. 1998; Berndt and Seyfried 1990) and studies of Li and B in geothermal systems (Reyes and Vickridge 1996) show that B partitions into aqueous fluids by a factor of ten compared to Li at 900 °C, and by a factor of greater than three at temperatures of 320–350 °C. However, at temperatures of <150 °C, the partitioning is almost equal. Under experimental conditions at low temperatures, B and Li were removed from seawater and incorporated into a dominantly smectite alteration phase, mirroring the situation in the Yax-1 impactites (Seyfried et al. 1984). The measured relative fractionation of Li and B between the different units is actually slightly greater for Li than B (Table 4). Our data are therefore consistent with a relatively low-temperature late-stage hydrothermal process, consistent with the observations that much of the alteration and vesicle filling occurred during the last stages of alteration of the impactites (e.g., Hecht et al. 2004). The low temperature indicated by the fractionation of Li and B and the difference in the major element abundances in the upper and lower units argue that protolith differences in the matrix materials in the Yaxcopoil-1 impactites, including primary and secondary carbonate components or both, are probably responsible for most of the differences in the mobile elements, although vertical transport cannot be ruled out. Additional data on the nature of the matrix materials, the bulk abundances of mobile trace elements, and stable isotopes will help constrain the nature of the postimpact hydrothermal processes in the Yaxcopoil-1 drill core.

CONCLUSIONS

Secondary ion mass spectrometry was used to determine the elemental contents of mobile trace elements in altered matrix materials from the Yaxcopoil drill core in the Chicxulub impact structure and the results provide evidence for mobile element variations that may be consistent with limited mobile element transport, but could also be due to variations in the protolith of the impactite matrix. The concentrations of the elements Li, B, and Be in the alteration material from the matrix of the impactite (Table 4) are enriched upward in the impactite sequence from Unit 5 to

Unit 2, as represented by samples from 862 m to 809 m, by factors of 3.5 (Li), 2.2 (B), and 1.5 (Be). The mobile elements Cs, Au, Rb, and Zn are enriched upward in the bulk analyses of Tuchscherer et al. (2004). Barium is depleted upward in the section, but the formation of barite in the impact breccias probably depleted the Ba concentrations in the fluids and therefore in the altered matrix materials in the upper units. The upward enrichments observed in the impactite section are consistent with the observed enrichments of mobile elements in the sediments immediately above the impact breccias (Rowe et al. 2004). Quantitative consideration of the mass of the mobile elements in the impact melt, the impact breccias, and the overlying sediments suggests that only a small fraction of the mobile elements from the impactites were deposited in the sediments directly above the impact breccias.

The relative fractionation of Li and B in the altered materials provides information on the temperature of the fluids involved in the formation of the late-stage altered matrix materials. Based on experimental data from the literature, the similar fractionation of Li and B in the impactites is consistent with a relatively low-temperature hydrothermal system during the formation of the altered matrix materials (<150 °C). The low temperature and relatively small amount of fractionation of the mobile elements is also consistent with the thin nature of the impactites at this location, which is probably not representative of the melt sheet within the transient cavity. Additional studies, including Li isotopes, may shed more light on the mobile element transport issues at this site.

The thin melt sheet at the Yax-1 location and the low temperature of the fluids implied by the trace element data may imply that only limited transport of mobile elements has occurred. In this case, the vertical variations in the major element composition of the altered matrix material must be due to different protolith compositions for this matrix material.

Acknowledgments–We wish to acknowledge the International Continental Drilling Program and the Chicxulub Scientific Drilling Project team for obtaining the Yax-1 core. We wish to thank Uwe Reimold, Phillipe Claeys, Christian Koeberl, and Doreen Ames for helpful reviews. Research was supported by the NASA Planetary Geology and Geophysics program.

Editorial Handling— Dr. Wolf Uwe Reimold

REFERENCES

Abramov O. and Kring D. A. 2004. Numerical modeling of an impact-induced hydrothermal system at the Sudbury crater *Journal of Geophysical Research* 109, doi:10.1029/2003JE002213.

Alvarez L. W., Alvarez W., Asaro F., and Michel H. V. 1980. Extraterrestrial cause for the Cretaceous/Tertiary extinction. *Science* 208:1095–1098.

Ames D. E., Watkinson D. H., and Parrish R. R. 1998. Dating of a regional hydrothermal system induced by the 1850 Ma Sudbury impact event. *Geology* 26:447–450.

Ames D. E., Kjarsgaard I. M., Pope K. O., Dressler B., and Pilkington M. 2004. Secondary alteration of the impactite and mineralization in the basal tertiary sequence, Yaxcopoil-1, Chicxulub impact crater, Mexico. *Meteoritics & Planetary Science* 39:1145–1167.

Berndt M. E. and Seyfried W. E., Jr. 1990. Boron, bromine, and other trace elements as clues to the fate of chlorine in mid-ocean ridge vent fluids. *Geochimica et Cosmochimica Acta* 54:2235–2245.

Brakenridge G. R., Newsom H. E., and Baker V. R. 1985. Ancient hot springs on Mars: Origins and paleoenvironmental significance of small Martian valleys. *Geology* 13:859–862.

Brenan J. M., Ryerson F. J., and Shaw H. F. 1998. The role of aqueous fluids in the slab-to-mantle transfer of boron, beryllium, and lithium during subduction: Experiments and models. *Geochimica et Cosmochimica Acta* 62:3337–3347.

Bridges J. C. and Grady M. M. 1999. A halite-siderite-anhydrite-chlorapatite assemblage in Nakhla: Mineralogical evidence for evaporites on Mars. *Meteoritics & Planetary Science* 34:407–415.

Bridges J. C. and Grady M. M. 2000. Evaporite mineral assemblages in the nakhlite (Martian) meteorites. *Earth and Planetary Science Letters* 176:267–279.

Bullock M. A., Moore J. M., and Mellon M. T. 2004. Laboratory simulations of Mars aqueous geochemistry. *Icarus* 170:404–423.

Claeys P., Heuschkel S., Lounejeva-Baturina E., Sanchez-Rubio G., and Stöffler D. 2003. The suevite of drill hole Yucatàn 6 in the Chicxulub impact crater. *Meteoritics & Planetary Science* 38: 1299–1317.

Dressler B. O., Sharpton V. L., Morgan J., Buffler R., Moran D., Smit J., Stöffler D., and Urrutia J. 2003. Investigating a 65 Ma old smoking gun: Deep drilling of the Chicxulub impact structure. *Eos* 84:125–130.

Dressler B. O., Sharpton V. L., Schwandt C. S., and Ames D. 2004. Impactites of the Yaxcopoil-1 drilling site, Chicxulub impact structure: Petrography, geochemistry, and depositional environment. *Meteoritics & Planetary Science* 39:857–878.

Dyar M. D., Wiedenbeck M., Robertson D., Cross L. R., Delaney J. S., Ferguson K., Francis C. A., Grew E. S., Guidotti C. V., Hervig R. L., Hughes J. M., Husler J., Leeman W., McGuire A. V., Rhede D., Rothe H., Paul R. L., Richards I., and Yates M. 2001. Reference minerals for the microanalysis of light elements. *Geostandards Newsletter* 25:441–463.

Förstner V. U. 1977. Geochemische Untersuchungen an den Sedimenten des Ries-Sees (Forschungsbohrung Nördlingen 1973). *Geologica Bavarica* 75:37–48.

Goto K., Tada R., Tajika E., Bralower T. J., Hasegawa T., and Matsui T. 2004. Evidence for ocean water invasion into the Chicxulub crater at the Cretaceous/Tertiary boundary. *Meteoritics & Planetary Science* 39:1233–1247.

Grew E. S., Chernosky J. V., Werding G., Abraham K., Marquez N., and Hinthorne J. R. 1990. Chemistry of kornerupine and associated minerals, a wet chemical, ion microprobe, and X-ray study emphasizing Li, Be, B and F contents. *Journal of Petrology* 31:1025–1070.

Grew E. S., Yates M. G., Shearer C. K., and Wiedenbeck M. 1997. Werdingite from Urungwe, Zimbabwe. *Mineralogical Magazine* 61:713–718.

Grew E. S., Yates M. G., Peacor D. R., Rouse R. C., McGee J. J., Huijsmans J. P. P., Shearer C. K., Wiedenbeck M., Thost D. E., and Su S.-C. 1998a. Boralsilite: A new borosilicate mineral related to sillimanite and its paragenesis in pegmatites. *American Mineralogist* 83:638–651.

Grew E. S., Yates M. G., Huijsmans J. P. P., McGee J. J., Shearer C. K., Wiedenbeck M., and Rouse R. C. 1998b. Werdingite, a borosilicate new to pegmatites. *Canadian Mineralogist* 36:399–414.

Grew E. S., Pertsev N. N., Vra'na S., Yates M. G., Shearer C. K., and Wiedenbeck M. 1998c. Kornerupine parageneses in whiteschist and other magnesian rocks: Is kornerupine + talc a high pressure assemblage equivalent to tourmaline + orthoamphibole? *Contributions to Mineralogy and Petrology* 131:22–38.

Grew E. S., Rao A. T., Raju K. K. V. S., Hejny C., Moore J. M., Waters D. J., Yates M. G., and Shearer C. K. 2003. Prismatine and ferrohogbomite-2N2S in granulite-facies Fe-oxide lenses in the Eastern Ghats Belt at Venugopalapuram, Vizianagaram district, Andhra Pradesh, India: Do such lenses have a tourmaline-enriched lateritic precursor? *Mineralogical Magazine* 67:1081–1098.

Hagerty J. J. and Newsom H. E. 2003. Hydrothermal alteration at the Lonar Lake impact structure, India: Implications for impact cratering on Mars. *Meteoritics & Planetary Science* 38:365–381.

Hawthorne F. C., Cooper M., Bottazzi P., Ottolini L., Ercit T. S., and Grew E. S. 1995. Micro-analysis of minerals for Boron by SREF, SIMS, and EMPA: A comparative study. *Canadian Mineralogist* 33:389–397.

Hecht L., Wittmann A., Schmitt R. T., and Stöffler D. 2004. Composition of impact melt particles and the effects of post-impact alteration in suevitic rocks at the Yaxcopoil-1 drill core, Chicxulub crater, Mexico. *Meteoritics & Planetary Science* 39: 1169–1186.

Herd C. D. K., Treiman A. H., McKay G. A., and Shearer C. K. 2002. Implications of experimental lithium and boron partition coefficients for the petrogenesis of Martian basalts (abstract). *Meteoritics & Planetary Science* 37:A62.

Herd C. D. K., Treiman A. H., McKay G. A., and Shearer C. K. 2004. The behavior of Li and B during planetary basalt crystallization. *American Mineralogist* 89:832–840.

Hervig R. L. 2002. Beryllium analyses by secondary ion mass spectrometry. In *Beryllium: Mineralogy, petrology, and geochemistry*, edited by Grew E. S. Washington, D.C.: Mineralogical Society of America. pp. 319–332.

Hildebrand A. R., Penfield G., Kring D. A., Pilkington M., Camargo A., Jacobson S. B., and Boynton W. V. 1991. A possible Cretaceous-Tertiary boundary on the Yucatán Peninsula, Mexico. *Geology* 19:867–871.

Kirsimae K., Suuroja S., Kirs J., Karki A., Polikarpus M., Puura V., and Suuroja K. 2002. Hornblende alteration and fluid inclusions in Kärdla impact crater, Estonia: Evidence for impact-induced hydrothermal activity. *Meteoritics & Planetary Science* 37:449–457.

Lentz R. C. F., Ryan J. G., Riciputi L. R., and McSween H. Y., Jr. 2000. Water in the Martian mantle: Clues from light lithophile elements in Martian meteorites (abstract #1672) 31st Lunar and Planetary Science Conference. CD-ROM.

Lentz R. C. F., McSween H. Y., Jr., Ryan J., and Riciputi L. R. 2001. Water in Martian magmas: Clues from light lithophile elements in shergottite and nakhlite pyroxenes. *Geochimica et Cosmochimica Acta* 65:4551–4565.

Lüders V. and Rickers K. 1994. Fluid inclusion evidence for impact-related hydrothermal fluid and hydrocarbon migration in cretaceous sediments of the ICDP-Chicxulub drill core Yax-1. *Meteoritics & Planetary Science* 39:1187–1197.

McCarville P. and Crossey L. J. 1996. Post-impact hydrothermal alteration of the Manson impact structure. In *The Manson impact structure, Iowa: Anatomy of an impact crater*, edited by Koeberl C. and Anderson R. R. Boulder, Colorado: Geological Society of America. pp. 347–376.

Moore D. M. and Reynolds R. C., Jr. 1997. *X-ray diffraction and the identification and analysis of clay minerals.* New York: Oxford University Press. 378 p.

Naumov M. V. 2002. Impact-generated hydrothermal systems: Data from Popigai, Kara, and Puchezh-Katunki impact structures. In *Impacts in Precambrian shields*, edited by Plado J. and Pesonen L. J. Berlin: Springer-Verlag. pp. 117–171.

Nelson M. J., Newsom H. E., and Draper D. S 2005. Incipient hydrothermal alteration of basalts and the origin of Martian soil. *Geochimica et Cosmochimica Acta* 69:2701–2711.

Nelson M. J. and Newsom H. E. 2006. Yaxcopoil-1 impact melt breccias: Silicate melt clasts among dolomite melt and implications for deposition (abstract #2081). 37th Lunar and Planetary Science Conference. CD-ROM.

Newsom H. E. 1980. Hydrothermal alteration of impact melt sheets with implications for Mars. *Icarus* 44:207–216.

Newsom H. E. and Hagerty J. J. 1997. Chemical components of the Martian soil: Melt degassing, hydrothermal alteration, and chondritic debris. *Journal of Geophysical Research* 102:19,345–19,355.

Newsom H. E., Graup G., Sewards T. and Keil K. 1986. Fluidization and hydrothermal alteration of the suevite impact melt deposit at the Ries crater, West Germany, and implications for Mars. *Journal of Geophysical Research* 91:E239–E251.

Newsom H. E., Hagerty J. J., and Goff F. 1999. Mixed hydrothermal fluids and the origin of the Martian soil. *Journal of Geophysical Research* 104:8717–8728.

Newsom H. E., Hagerty J. J., and Thorsos I. E. 2001. Location and sampling of aqueous and hydrothermal deposits in Martian impact craters. *Astrobiology* 1:71–88.

Osinski G. R., Spray J. G., and Lee P. 2001. Impact-induced hydrothermal activity within the Haughton impact structure, arctic Canada: Generation of a transient, warm, wet oasis. *Meteoritics & Planetary Science* 36:731–745.

Osinski G. R., Lee P., Parnell J., Spray J. G., and Baron M. 2005. A case study of impact-induced hydrothermal activity: The Haughton impact structure, Devon Island, Canadian High Arctic. *Meteoritics & Planetary Science* 40:1859–1877.

Ottolini L. and Hawthorne F. C. 2001. An investigation of SIMS matrix effects on H, Li, and B ionization in tourmaline. *European Journal of Mineralogy* 11:679–690.

Ottolini L., Bottazzi P., and Vannucci R. 1993. Quantification of lithium, beryllium, and boron in silicates by secondary-ion mass-spectrometry using conventional energy-filtering. *Analytical Chemistry* 65:1960–1968.

Paul R. L. 2005. Determination of boron in materials by cold neutron prompt gamma-ray activation analysis. *The Analyst* 130:99–103.

Pearce J. G., Perkins W. T., Westgate J. A., Gorton M. P., Jackson S. E., Neal C. R., and Chenery S. P. 1997. A compilation of new and published major and trace element data for NIST SRM 610 and NIST SRM 612 glass reference materials. *Geostandards Newsletter* 21:115–144.

Pope K. O. 2002. Impact dust not the cause of the Cretaceous-Tertiary mass extinction. *Geology* 30:99–102.

Puura V., Huber H., Kirs J., Karki A., Suuroja K., Kirsimae K., Kivisilla J., Kleesment A., Konsa M., Preeden U., Suuroja S., and Koeberl C. 2004. Geology, petrography, shock petrography, and geochemistry of impactites and target rocks from the Kärdla crater, Estonia. *Meteoritics & Planetary Science* 39:425–451.

Reyes A. G., and Vickridge I. C. 1996. Distribution of lithium, boron and chloride between fresh and altered rocks in the Kawerau geothermal system, New Zealand. Proceedings, 18th New Zealand Geothermal Workshop. pp. 121–126.

Rocholl A., Dulski P., and Raczek I. 2000. New ID-TIMS, ICP-MS,

and SIMS data on the trace element composition and homogeneity of NIST certified reference material SRM 610–611. *Geostandards Newsletter* 24:261–274.

Rowe A. J., Wilkinson J. J., Coles B. J., and Morgan J. V. 2004. Chicxulub: Testing for post-impact hydrothermal input into the Tertiary ocean. *Meteoritics & Planetary Science* 39:1223–1231.

Seyfried W. E., Jr., Janecky D. R., and Mottl M. J. 1984. Alteration of the oceanic crust: Implications for geochemical cycles of lithium and boron. *Geochimica et Cosmochimica Acta* 48:557–569.

Shimizu N. and Hart S. R. 1982. Applications of the ion microprobe to geochemistry and cosmochemistry. *Annual Review of Earth and Planetary Science* 10:483–526.

Stöffler D., Artemieva N. A., Ivanov B. A., Hecht L., Kenkmann T., Schmitt R. T., Tagle R. A., and Wittmann A. 2004. Origin and emplacement of the impact formations at Chicxulub, Mexico, as revealed by the ICDP deep drilling at Yaxcopoil-1 and by numerical modeling. *Meteoritics & Planetary Science* 39:1035–1067.

Taylor S. R. and McLennan S. M. 1985. *The continental crust: Its composition and evolution.* Oxford: Blackwell Scientific. 312 p.

Teng F. Z., McDonough W. F., Rudnick R. L., Dalpe C., Tomascak P. B., Chappell B. W., and Gao S. 2004. Lithium isotopic composition and concentration of the upper continental crust. *Geochimica et Cosmochimica Acta* 68:4167–4178.

Tuchscherer M. G., Reimold W. U., Koeberl C., Gibson R. L., and de Bruin D. 2004. First petrographic results on impactites from the Yaxcopoil-1 borehole, Chicxulub structure, Mexico. *Meteoritics & Planetary Science* 39:899–930.

Tuchscherer M. G., Reimold W. U., Koeberl C., and Gibson R. L. 2005. Geochemical and petrographic characteristics of impactites and Cretaceous target rocks from the Yaxcopoil-1 borehole, Chicxulub impact structure, Mexico: Implications for target composition. *Meteoritics & Planetary Science* 40:1513–1536.

Wallace P. and Carmichael I. S. E. 1992. Sulfur in basaltic magmas. *Geochimica et Cosmochimica Acta* 56:1863–1874.

Zürcher L. and Kring D. A. 2004. Hydrothermal alteration in the core of the Yaxcopoil-I borehole, Chicxulub impact structure, Mexico. *Meteoritics & Planetary Science* 39:1199–1221.